PERGAMON

International Journal of Heat and Mass Transfer 45 (2002) 5053–5067

International Journal of HEAT and MASS TRANSFER

www.elsevier.com/locate/ijhmt

Energetic budget on an evaporating monodisperse droplet stream using combined optical methods Evaluation of the convective heat transfer

G. Castanet [a], P. Lavieille [a], F. Lemoine [a,*], M. Lebouché [a], A. Atthasit [b], Y. Biscos [b], G. Lavergne [b]

[a] *LEMTA—UMR 7563, ENSEM, 2 Avenue de la Forêt de Haye, B.P. 160, F-54504 Vandœuvre-les-Nancy Cedex, France*
[b] *ONERA-DMAE, Centre de Toulouse, B.P. 4025, 31055 Toulouse Cedex, France*

Received 24 January 2002; received in revised form 27 March 2002

Abstract

Aerothermal properties in a fuel spray is a central problem in the field of the design of the combustion chambers of automotive engines, turbojets or rocket engines. Heat and mass transfer models are necessary in the predictive calculation schemes used by the motorists. Reliable experimental data must be obtained for both the validation and development of new physical models linked to heat transfer and evaporation in sprays, where aerodynamic interactions have a key role. This paper proposes an experimental study of the energetic budget of a monodisperse ethanol droplet stream, injected in the thermal boundary layer of a vertical heated plate. The droplet size reduction is measured using a light scattering technique (interferential method) in order to characterize the evaporation, as the droplet mean temperature is monitored using the two colors laser-induced fluorescence technique. The convection heat transfer coefficient and the Nusselt number are inferred from the overall energetic budget, as a function of the inter-droplet distance, characterizing the interaction regime. The results are compared to physical models combined with numerical simulations available in the literature, for moving, evaporating isolated droplets and for three droplets arrangement in linear stream.

1. Introduction

The knowledge of the aerothermal properties of the spray is a central problem for the design of modern combustion chambers of turbojets, automotive engines and rockets engines. The fuel is injected into the combustion chamber by high pressure atomizers as a liquid spray. The fuel spray is composed of individual liquid droplets ranging from a few μm to a few 100 μm in diameter, with velocities of a few 10 $m\,s^{-1}$. Predictive capabilities of the large calculation codes would benefit from a better understanding of the highly complex phenomena occurring during all the phases of the spray combustion. For dense spray, the evaporation model appears clearly one of the key point, since it is directly related to the specific consumption of the engine and to the pollutant formation.

During the expansion of the spray in the combustion chamber, air is entrained by viscous effects, leading to the mixture between the vaporized fuel and the oxidizer. Evaporation and combustion models of isolated, stagnant or moving fuel droplets are well described in the literature [1,2]. Close to the injector, the interaction phenomena between the droplets themselves and with the entrained vapor phase are strong and predominant and therefore cannot be neglected, as demonstrated in numerous papers [3–7]. In evaporation and combustion problems, the heat transfer between the hot gaseous

* Corresponding author. Tel.: +33-03-83-59-57-32; fax: +33-03-83-59-55-44.
E-mail address: flemoine@ensem.inpl-nancy.fr (F. Lemoine).

0017-9310/02/$ - see front matter
PII: S0017-9310(02)00204-1

Nomenclature

C	distance parameter, $C = L/D_d$
C_p	fuel specific heat (at constant pressure) ($J\,kg^{-1}\,K^{-1}$)
D_d	droplet diameter (m)
h	specific enthalpy ($J\,kg^{-1}$)
L	inter-droplet distance (center to center)
L_v	liquid fuel latent heat of vaporization ($J\,kg^{-1}$)
m	droplet mass (kg)
Pr	Prandtl number
Re	Droplet Reynolds number
S	droplet surface (m^2)
T_∞	temperature in the hot plate boundary layer (K)
T_{ref}	reference temperature (K)
$V(t)$	droplet volume (m^3)
V_d	droplet velocity ($m\,s^{-1}$)
T_m	mean droplet temperature (K) defined by $T_m = 1/m \int_{V(t)} \rho T\,dV$
Y	fuel mass fraction in the gaseous phase

Greek symbols

Φ_c	convective heat flux (W)
Φ_{vap}	vaporization heat flux (W)
β	temperature sensitivity of the fluorescence intensity (K)
Φ	total heat flux extracted from the droplets (W)
φ	total heat flux density (per unit of surface) extracted from the droplets ($W\,m^{-2}$)
λ	thermal conductivity ($W\,m^{-1}\,K^{-1}$)
λ_{eff}	effective thermal conductivity ($W\,m^{-1}\,K^{-1}$)
ρ	specific density ($kg\,m^{-3}$)
ρ_v	vapor fuel specific density ($kg\,m^{-3}$)
σ	molecular diffusivity of the ethanol vapor ($m^2\,s^{-1}$)

Subscripts

g	fuel gas phase
l	fuel liquid phase
ref	reference state

phase and the liquid fuel droplets is a central point of interest, since it both depends on the fuel and gas phase physical properties and aerodynamic interaction phenomena, especially for the liquid mass fraction encountered in this application area. The high degree of complexity of these phenomena and the large number of droplets to be considered, makes that the direct computation of the Navier–Stokes and energy equations requires too calculations steps and time.

The thermal and aerodynamic interactions between droplets must be modeled using global parameters of the two phases. Experimental data are necessary in order to establish and validate models or correlations. When a droplet is moving in a hot gas environment, thermal energy is transferred to the droplet by forced convection: a part of this energy is used for the droplet heating by diffusion in the liquid phase and the other part for evaporation. Very few information exists about the forced convection and heat transfer coefficient. Chiang and Sirignano [5], with the use of numerical simulation, determined correlations of the Nusselt and Sherwood numbers of evaporating and combusting moving droplets, as a function of the inter-droplet distance, for three droplets in linear stream. On the other hand, experimental data must be collected in sufficiently basic and realistic situations. Monodisperse droplets in linear stream are a good example for which the influence of different parameters such as drop size, velocity, inter-droplets distance and gas phase temperature can be easily separated.

The present works deals with an experimental study of a monodisperse ethanol droplet stream injected in the thermal boundary layer of a heated vertical plate. The global enthalpy gained by the jet is measured by the mean droplet temperature temporal evolution. Energy loss by evaporation is monitored by the droplets size reduction measurement. The energy budget over the evaporating droplet allows to infer the energy gained by forced convection as a function of the interaction regime modified by changing the inter-droplet distance. The associated heat transfer coefficient and Nusselt number have been calculated and compared to some data available in the literature. The droplet size and mean droplet temperature evolutions are necessary in order to evaluate this energetic budget. The measurement of elastically scattered radiation from a spherical droplet in the forward direction, also referred in the literature as an interference technique allow to determine with high accuracy the droplet size [7,8], and will be used in the present work. The two colors laser-induced fluorescence initiated by Lavieille et al. [9] has been used and allows accurate mean droplet temperature measurements to be performed. The technique uses fuel (ethanol in the present case) doped with a fluorescent organic dye at low concentration, the rhodamine B, which should not vaporize as well as the fuel. The techniques provides the mean temperature with an accuracy better than 1 °C, and remains unbiased by the droplet internal temperature gradients and by non-sphericity, differently from the rainbows techniques [10].

2. Experimental set-up

2.1. Droplet generation

A linear monodisperse droplet stream is generated by Rayleigh disintegration of a liquid jet [8], with the use of a mechanical vibration obtained by a piezoceramic, excited by a square wave. The applied voltage on the piezoceramic depends on the desired position of the break-up zone and on the fuel physical properties, related to the injection temperature. For a particular frequency range, the liquid jet breaks into equally spaced and monosized droplets, at the frequency of the forced mechanical vibration. The liquid fuel (ethanol here) is pressurized with compressed air and is forced through a calibrated orifice ranging from $\Phi_0 = 50$ μm to $\Phi_0 = 100$ μm in diameter. According to Rayleigh theory, the resulting droplet diameter is about 1.9 Φ_0. The droplet injection velocity can range from 2 $m\,s^{-1}$ to about 10 $m\,s^{-1}$. The fuel can be pre-heated in the injector body by means of a thermostated external water circulation, up to its boiling point. The temperature of the fuel is measured exactly at the injection point with the use of a K type thermocouple. The frequency range for which a monodisperse jet can be obtain is very limited around the frequency given by the Raleigh theory. A technique of electrostatic deviation of the droplet has been implemented in order to adjust the droplets spacing, without changing the droplet diameter. The deviator is mounted at the injector exit (Fig. 1). The stream passes through a ring charged by positive electrical impulses, positioned just at the break-up location of the cylindrical jet so that the droplets can be negatively charged by electrical impulses transmitted by the ring. Consequently, a periodically selected number of droplets can acquire a negative electrical charge. After being charged, the droplets are streaming between two plates where a high intensity electrostatic field is created. The charged droplets are deviated on the side of the positive plate and picked up. The rest of the jet is undeviated and presents a different droplet spacing from the initial jet, depending on the number of the initially charged droplets. With the use of this device, 2/3, 3/4, 4/5 droplets or more can be eliminated as shown in the picture of the Fig. 1.

In these experiments, ethanol has been used as a fuel, because it is a single component fuel, which greatly simplified the fundamental analysis of heat transfers. Furthermore, the physical properties of this compound are stable and well characterized.

2.2. Evaporation device

The monodisperse droplet stream is injected in the thermal free convection boundary layer of a vertical heated plate. The plate is built in ceramic and contains near its surface an electrically heated wire. The electrical power dissipated in the wire is about 200 W. The heat flux dissipated by free convection over one side of the plate is about 13 W. The resulting estimated thermal boundary layer thickness is about 8 mm at 5 mm from

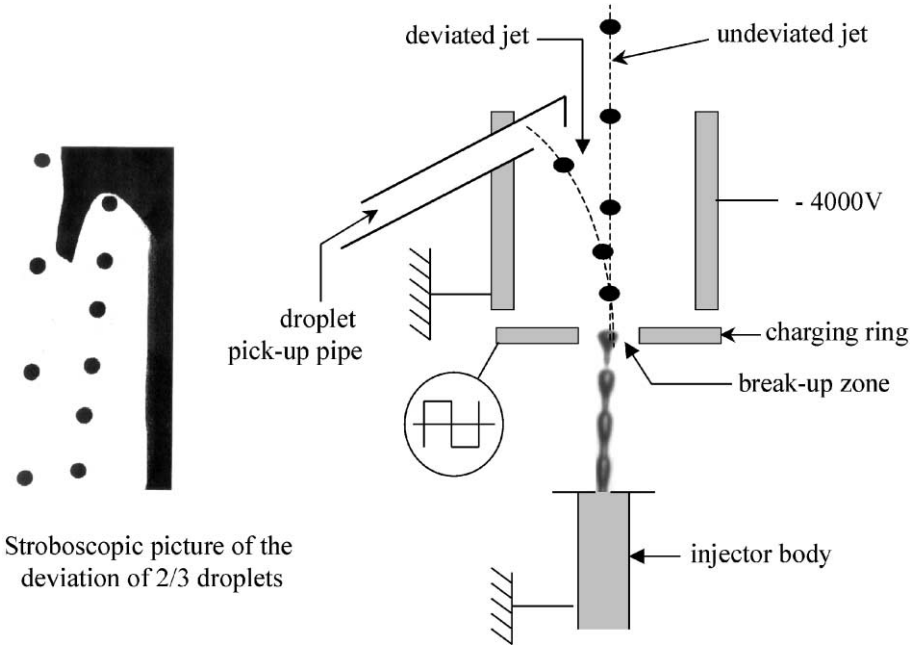

Fig. 1. Electrostatic deviation principles.

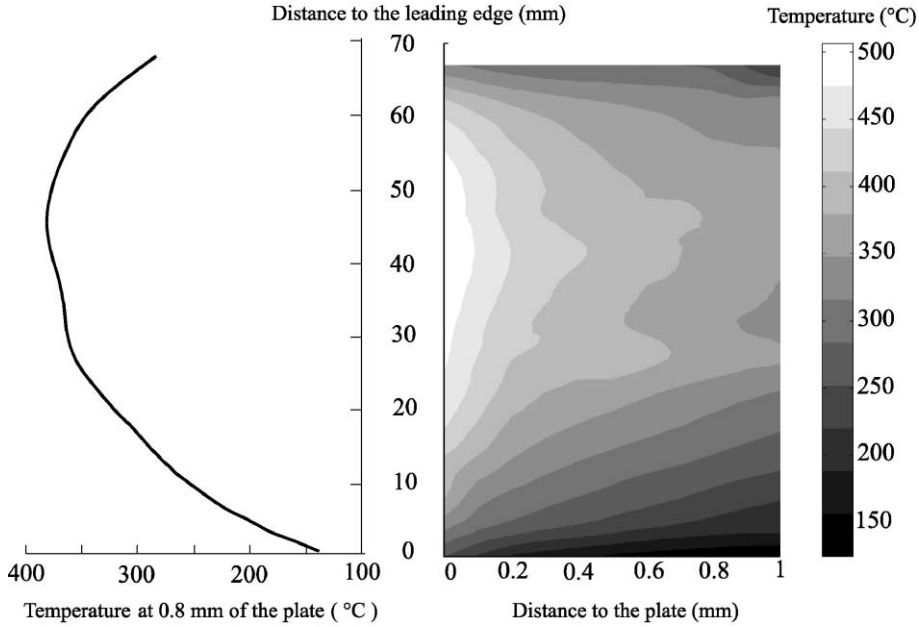

Fig. 2. Thermal hot plate boundary layer temperature measurement.

the leading edge of the plate and 12 mm at 60 mm. The temperature field in the plate boundary layer, measured by a K thermocouple (20 μm in diameter at the junction), is presented in the Fig. 2. The thermocouple is mounted on a 3D traverse device, in the direction of the isothermal lines. The temperature distribution corresponds to a natural convection thermal boundary layer. The boundary effects can be observed, since a noticeable temperature decrease is visible in the trailing edge of the plate. The monodisperse stream axis is adjusted strictly in the parallel direction of the plate, in the middle. The droplet diameter used is 105 μm at the injection point and the stream axis is positioned at 800 μm from the heated plate surface (Fig. 3). The temperature profile in the thermal boundary layer, at 800 μm from the plate is also reported in the Fig. 2. The injection velocity is about 8 $m\,s^{-1}$. The experimental device can be seen on the Fig. 3. The droplet stream can be visualized by means of a rapid stroboscopic device synchronized with a CCD camera equipped with a high magnification optical set-up. With the use of this system, the monodisperse character of the stream can be checked.

3. Experimental techniques

3.1. Droplet diameter reduction measurement

The knowledge of the droplet diameter reduction is necessary in order to characterize the evaporation. The measurement technique is based on the interaction between a spherical droplet and a laser beam [8,11]. A laser beam, issuing from an argon ion laser is focused on a droplet (Fig. 4). The order 0 and 1 refracted rays, generate an interference pattern in the forward direction. The high frequency of the droplets production makes that the fringe pattern appears stationary. The intensity distribution of the scattered light is described by Mie's theory, according to the value of the Mie parameter:

$$\alpha = \frac{\pi D_d}{\lambda} \tag{1.1}$$

where D_d is the droplet diameter and λ the laser wavelength.

For $\alpha \gg 1$, $\alpha \approx 640$ in the present case, the equations of the geometrical optics can be used instead of the Mie theory, in order to determine the light intensity distribution. These simplifications allow a correct description of the fringe pattern for scattering angles between 30° and 80° in the forward direction. The measurement of the angular inter-fringe $\Delta\theta$ for a forward scattering angle θ allows to determine the droplet diameter following the relation:

$$D_d = \frac{2}{\Delta\theta\left(\cos\left(\frac{\theta}{2}\right) + n\sin\left(\frac{\theta}{2}\right)\Big/\sqrt{1-2n\cos\left(\frac{\theta}{2}\right)+n^2}\right)} \tag{1.2}$$

where n is the liquid refraction index. The refraction index is temperature dependent, but the influence of the refraction index on the diameter measurement is very

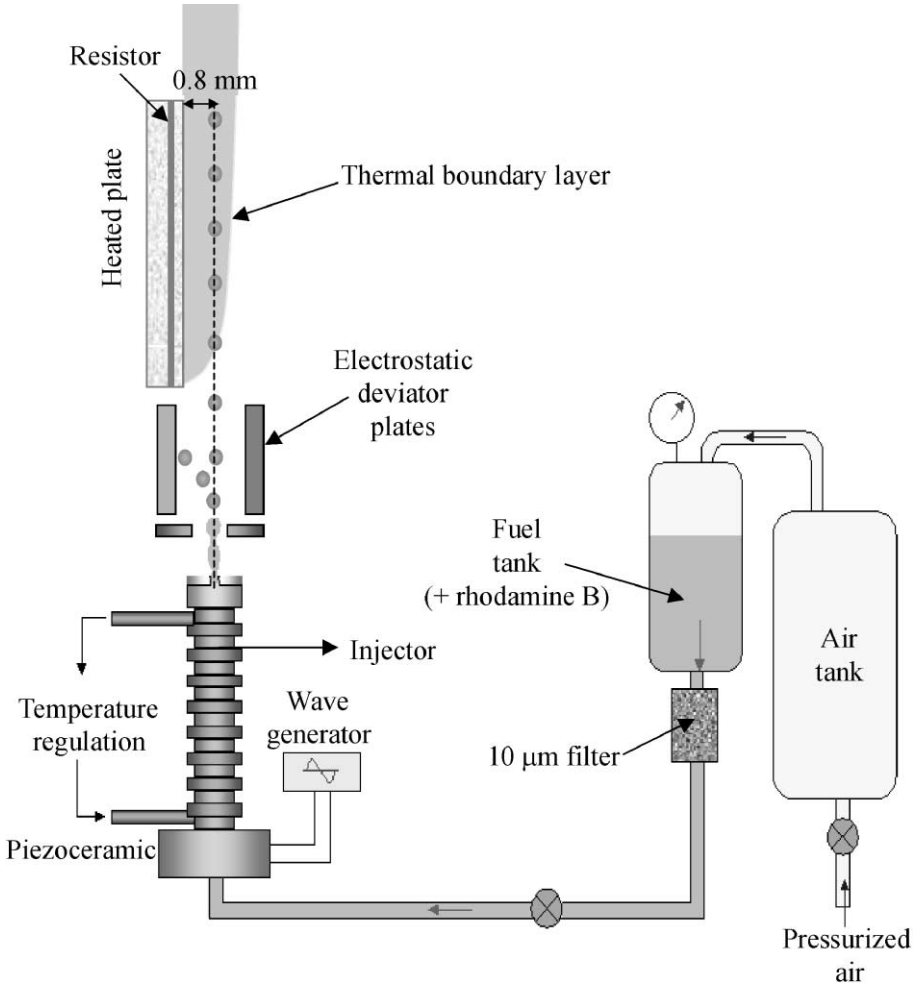

Fig. 3. Experimental arrangement.

limited [12]. The optical signal is recorded on a linear CCD camera on 2048 pixels (Fig. 4) and the auto-correlation of this signal is calculated in order to eliminate the background noise (see the auto-correlation in the bottom Fig. 4). The angular spacing is measured between two interference maxima in order to calculate the droplet size. According to the uncertainties on the geometrical parameters and liquid refraction index, the absolute error on the diameter determination is about 1.5%; however, the relative size variation measurement accuracy is expected to be far better.

3.2. Droplet temperature measurement

The droplet temperature evolution is also necessary in order to complete the evaporating droplet thermal budget. The technique used is the two colors laser-induced fluorescence, and the main principles of this technique are detailed in this section. All the technical details can be found in Lavieille et al. [9]. The fuel, ethanol here, should be previously seeded with a low concentration (a few ppm) of rhodamine B, which is a fluorescent dye very sensitive to the temperature. The rhodamine B fluorescence can be easily induced by the green line ($\lambda = 514.5$ nm) of the argon ion laser. The rhodamine B fluorescence spectrum is broadband, and it has been shown that its temperature sensitivity was strongly depending on the wavelength. This temperature dependency follows Eq. (1.3) [9,13]:

$$I_f = K_{opt} K_{spec} V_c I_0 C e^{\beta(\lambda)/T} \tag{1.3}$$

where K_{opt} is an optical constant, K_{spec} is a constant depending solely on the spectroscopic properties of the fluorescent tracer, I_0 the laser excitation intensity, C the molecular tracer concentration, T the absolute temperature and V_c the fluorescence photons collection volume.

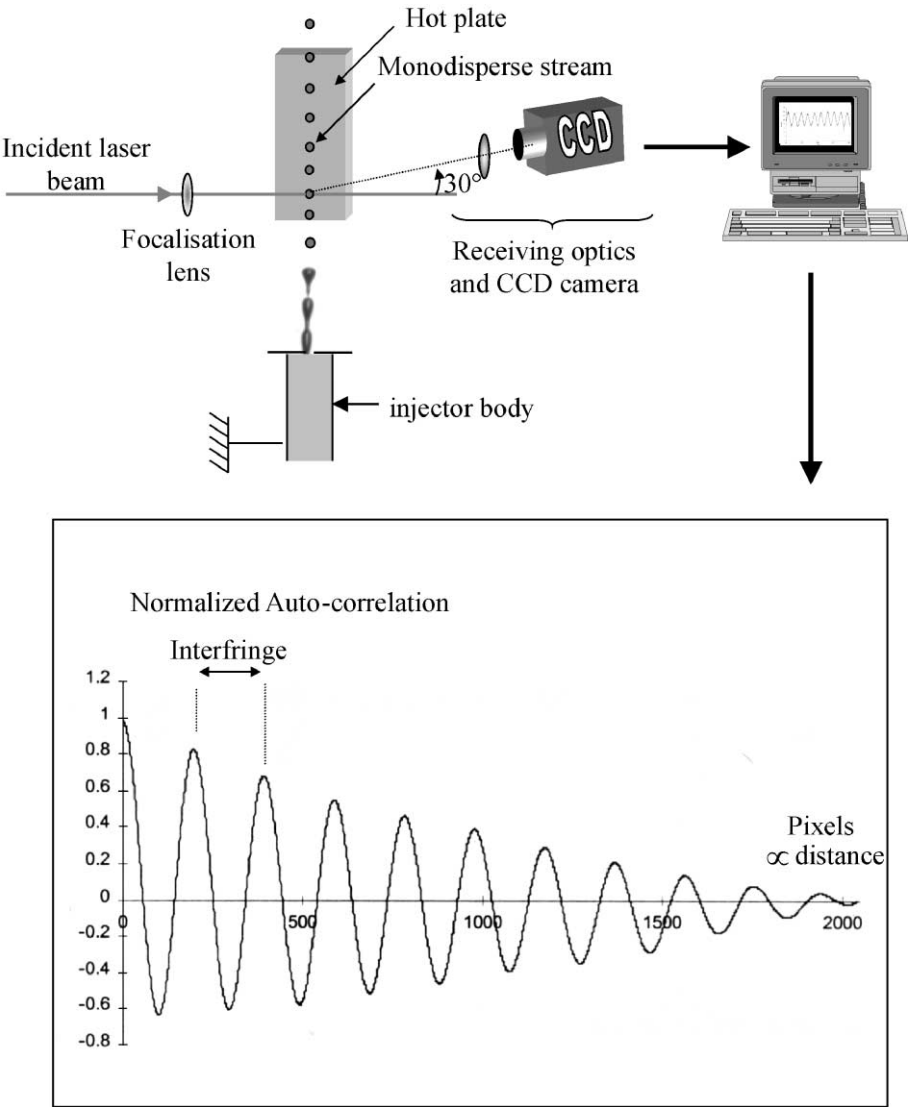

Fig. 4. Droplet size measurement by the interference method.

The product CV_c of the collection volume by the tracer molecule concentration corresponds to the number of rhodamine B molecules excited by the laser radiation and observed by the photodetector. This parameter is strongly related to the drop size and to the probe volume dimensions. The parameter $\beta(\lambda)$ characterizes the temperature dependence on the wavelength λ. One of the main problem for measuring the temperature via the fluorescence intensity is the triple dependence of the fluorescence signal on temperature, number of excited molecules and laser intensity. The solution found is to detect the fluorescence signal simultaneously on two spectral bands. The averaged temperature sensitivity coefficients on these two bands are denoted by β_1 and β_2.

The ratio R_f of the fluorescence signals measured on each spectral band is given by:

$$R_f = \frac{I_{f1}}{I_{f2}} = \frac{K_{opt1}}{K_{opt2}} \frac{K_{spec1}}{K_{spec2}} e^{\frac{\beta_1 - \beta_2}{T}} \tag{1.4}$$

This ratio is totally independent on the collection volume of the fluorescence signal, on the droplet size, on the laser excitation intensity and on the tracer concentration and depends only on temperature. The use of a single reference point where the temperature is known, e.g. the injection point, allows to eliminate the system dependence, i.e. the constants depending on optics and spectroscopy. The position of the two detection spectral bands is optimized in order to maximize the difference

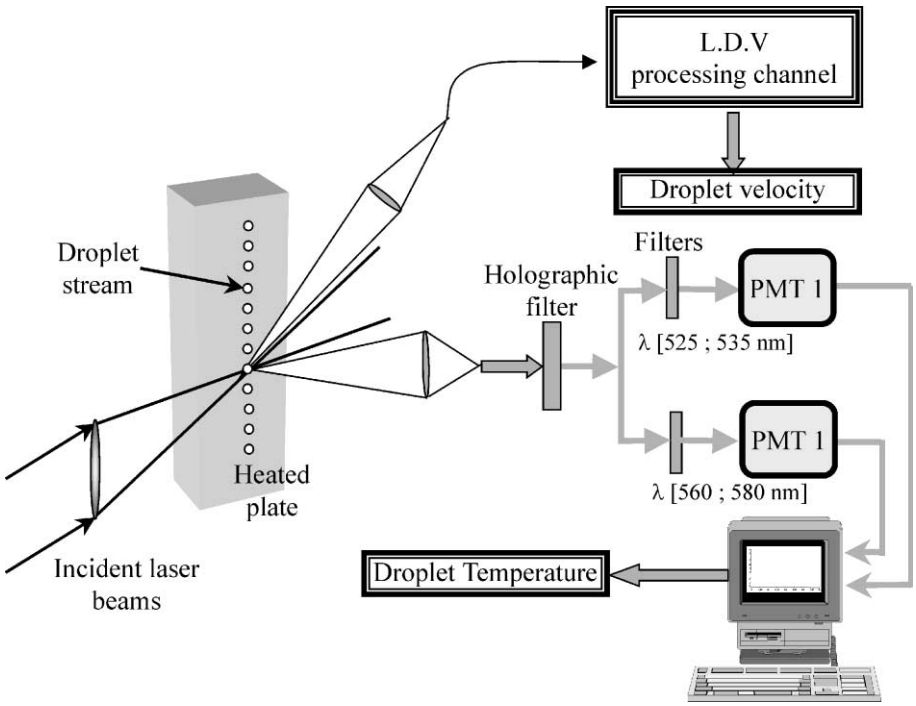

Fig. 5. Two colors laser-induced fluorescence experimental set-up.

$(\beta_1 - \beta_2)$. The resulting temperature sensitivity is about 2%/K and 0.5 °C temperature variations appear detectable.

Two intersecting laser beams issuing from the same laser source have been used in order to create the probe volume (Fig. 5). This optical configuration allows to measure concomitantly the droplet velocity by Laser Doppler Velocimetry and subsequently the time elapsed from the injection point, since the droplet stream is stationary. If L_i is the distance from the injection point at the i^{th} point, and t_i the time for covering the distance L_i, then t_{i+1} is calculated by:

$$t_{i+1} = t_i + \frac{L_{i+1} - L_i}{(V_{i+1} + V_i)/2}$$

where V_i is the velocity measured at the i^{th} point. The measuring volume dimensions for the fluorescence signal are given by the product of the excitation field by the detection field of view, corresponding to ($115 \times 115 \times 150$ μm), which are higher than the droplet diameter. Furthermore, the fluorescence signal is averaged on the overall transit of the droplet in the probe volume, so as a space averaged temperature over the droplet can be determined. The fluorescence signal is collected at right angle. A set of beamsplitters and optical filters allows to eliminate the laser scattering on the droplets and to divide the fluorescence signal into the two specified spectral bands, as indicated by Lavieille et al. [9]. Optical signal corresponding to each spectral band are detected and converted into analog voltages by two parallel photomultipliers equipped with pre-amplifiers.

4. Experimental results and discussion

4.1. Droplet size reduction and temperature measurements

The interaction regime can be expressed by the distance parameter C, defined by the ratio between the inter-droplet distance and the droplet diameter. A large range of distance parameters is explored, between 2.6 and 16.2 and all the considered distance parameters are defined at the injection point. However the diameter reduction for $C = 16.2$ appeared difficult to exploit due to the trajectory instability of the droplets. The squared diameter is presented in the Fig. 6 as a function of the time elapsed from the leading edge of the plate, for the different investigated distance parameters. The measured droplet diameters have been corrected from the thermal expansion phenomena, by taking into account the ethanol specific density variation with the measured temperature in order to keep D_d^3 proportional to the droplet mass. The droplet size reduction rate increases strongly with the distance parameter: it is about 1.7% for $C = 2.6$ and 13.5% for $C = 13.9$ between 3 and 10 ms,

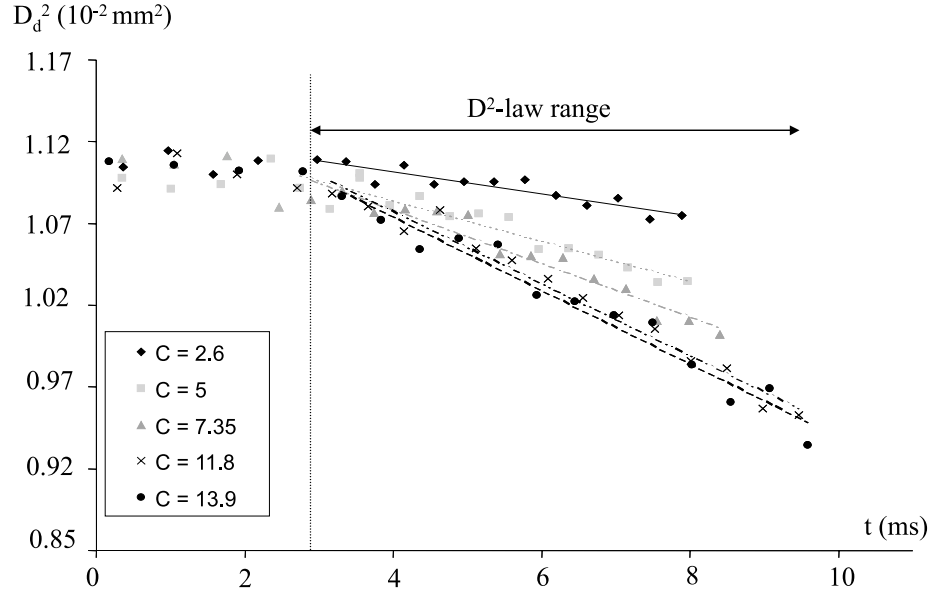

Fig. 6. Droplet diameter measurements.

corresponding to a mass loss of 5% and 36% respectively. Two main phases can be distinguished in the evaporation process: a first phase (from $t = 0$ to 3 ms) where the size reduction is low and the distance parameter influence is very low. Beyond this point, the evaporation is more intense and follows the modified D^2 law [2,14–16] according to the relation:

$$D_d^2 = D_{d0}^2 - \eta K' t \tag{1.5}$$

The influence of the distance parameter appears also well marked and will be discussed in the Section 4.3. The factor η ($0 < \eta < 1$) takes into account the interaction phenomena and depends only on the distance parameter and will be calculated in the light of the experimental data. The parameter K', taking into account the convective heat transfer between the droplet and its gaseous environment, represents the squared diameter decreasing rate for an isolated droplet in motion calculated using the Ranz–Marshall correlation [15]:

$$K' = \left(1 + 0.3\sqrt{Re_{ref}} Pr_{ref}^{1/3}\right) \frac{8\rho_g \sigma}{\rho_l} \ln(1 + B_T) \tag{1.6}$$

where B_T is the Spadling number calculated by:

$$B_T = \frac{C_{pg}(T_\infty - T_S)}{L_v} \tag{1.7}$$

The Reynolds and Prandtl numbers and the gas phase properties i.e. ρ_g, C_{pg}, σ are calculated in the reference state defined accordingly to the "1/3" law rule [17]:

$$T_{ref} = T_S + \tfrac{1}{3}(T_\infty - T_S) \tag{1.8}$$

and

$$Y_{ref} = Y_S + \tfrac{1}{3}(Y_\infty - Y_S) \tag{1.9}$$

As the droplet surface temperature T_S is unknown, the droplet mean temperature, measured by two colors LIF is used. The temperature T_∞ corresponds to these measured by the thermocouple, in the thermal boundary layer of the heated plate, by averaging the temperature at the left and right droplet stream boundaries. The fuel mass fraction at the droplet surface Y_S is calculated at the saturation conditions [1] and Y_∞ is null.

With the calculation of K' according to the Ranz–Marshall correlation, and the slope of the D_d^2 temporal evolution, the factor η has been evaluated as function of the distance parameter. The variation of η as a function of the distance parameter is presented in the Fig. 7. For each initial distance parameter, the entire variation range of the distance parameter along the jet, due to the velocity reduction caused by the drag force, is represented. A mean curve is drawn along with the results of Virepinte [6] obtained for a monodisperse ethanol droplet stream in combustion, and for similar aerothermal conditions than in the present work. The influence of the interaction phenomena appears strong between $C = 2$ and 6 and is decreasing after. It can be also noted that the results obtained in simple evaporation are similar to those

[1] $Y_S = P_S(T_S)/P_a$ and $P_S(T_S) = 133.2e^{(18.9119-3803;98/T-41.68)}$ for ethanol (T: absolute liquid fuel temperature, P_a: atmospheric pressure).

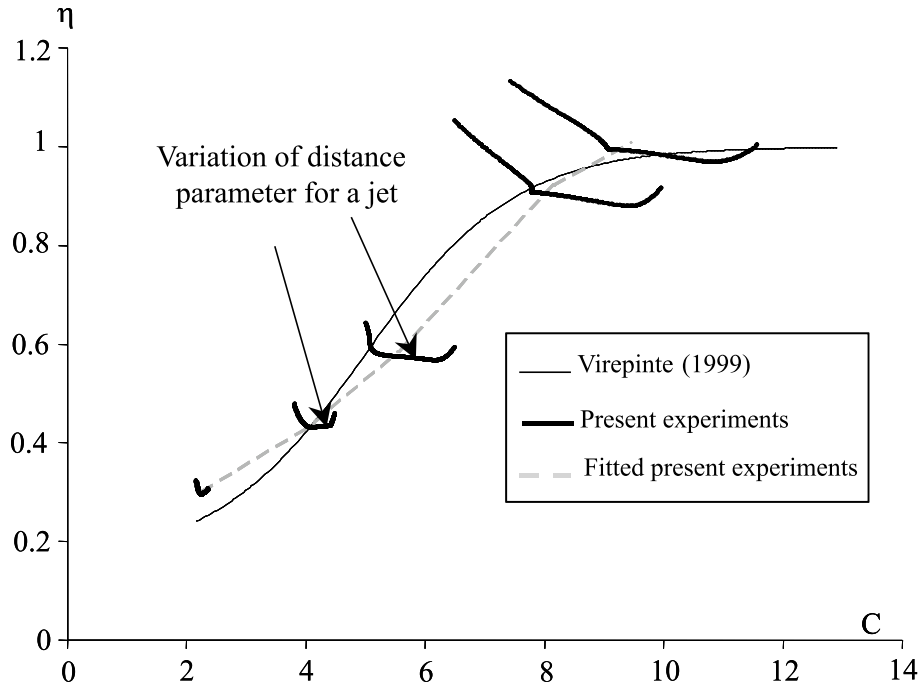

Fig. 7. Correction factor for the modified D^2-law.

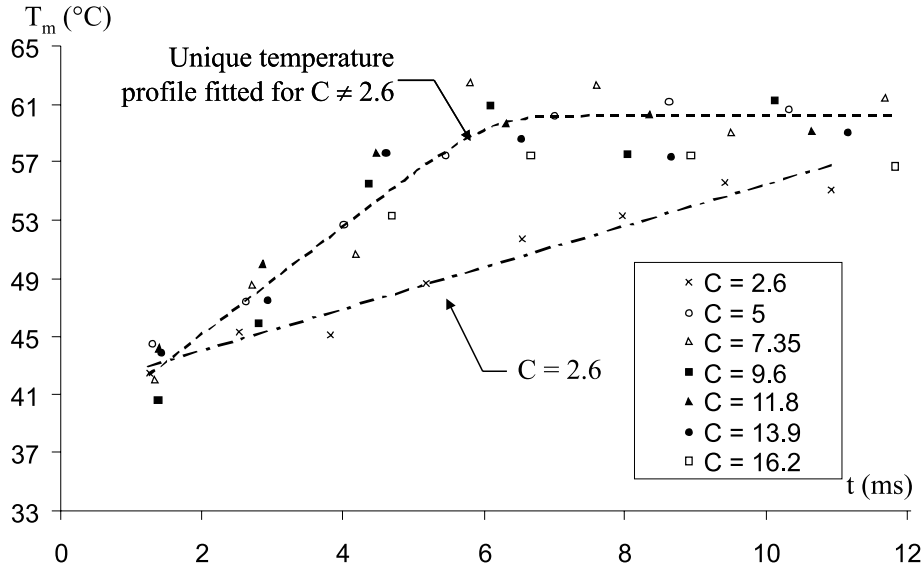

Fig. 8. Droplet mean temperature measurements.

obtained in combustion by Virepinte [6] and appear therefore universal for evaporating droplets.

The mean droplet temperature temporal evolution is presented in the Fig. 8, for each explored distance parameters. Except for the smallest distance parameter ($C = 2.6$), the temperature increases regularly during about 5 ms, before reaching an equilibrium temperature at about 60 °C. The influence of the different tested distance parameters cannot be clearly distinguished for $C \geqslant 5$, which will be discussed in the Section 4.3. For the case $C = 2.6$, as seen in the Fig. 8, the temperature increase is slower and the equilibrium temperature is not

reached before the top of the plate. Additional measurements would be useful in the range between $C = 2.6$ and 5, but are impossible to perform with the electrostatic deviator. The only issue is to modify the piezoceramic frequency, but the droplet size would be also changed and the subsequent interpretation would be biased. However, the cases corresponding to this strong interaction regime are rarely encountered in the engine applications.

4.2. Energetic budget

The droplet enthalpy evolution is directed by the variation of the heat fluxes resulting from forced convection with the gaseous environment, vaporization and radiation. The radiation effects are often neglected in the budget [18,19], since the droplets are supposed to behave as a transparent medium. Heat exchanges operate at the droplet surface and the heat is diffused in the liquid phase by conduction and convection, helped by the formation of internal motions. The case of a moving evaporating droplet, with a regressing surface will be considered. Assuming that the local heat flux exchanged at the droplet surface is homogeneous, the overall budget equation can be summarized by:

$$\underbrace{mC_{pl}\frac{\mathrm{d}T_{\mathrm{m}}}{\mathrm{d}t}}_{(a)}+\underbrace{C_{pl}(T_{\mathrm{m}}-T_{\mathrm{S}})\frac{\mathrm{d}m}{\mathrm{d}t}}_{(b)}=\Phi_{\mathrm{c}}+\Phi_{\mathrm{vap}} \tag{1.10}$$

where T_{S} is the droplet surface temperature, Φ_{c} is the convective heat flux exchanged with the gaseous environment and Φ_{vap} is the vaporization heat flux defined by:

$$\Phi_{\mathrm{vap}}=L_{\mathrm{v}}\frac{\mathrm{d}m}{\mathrm{d}t} \tag{1.11}$$

The term (a) corresponds to the droplet heating flux, and (b) to the loss of enthalpy flux due to the surface regression caused by the evaporation.

4.3. Convective heat transfer characterization

Each terms of the Eq. (1.10) can be evaluated with the experimental data. The term (b) be can be overestimated by taking the highest temperature for the surface temperature T_{S}: it remains at least 40 times less than the other fluxes and will be therefore neglected. The term (a) is evaluated by calculating the derivate the fitted temperature profiles obtained for the different distance parameters. The vaporization flux Φ_{vap} is determined by derivating droplet mass temporal evolution, according to the experimental data fitted by the modified D^2 law (Eq. (1.5)). The convective heat flux is deduced through the overall budget (Eq. (1.10)). The temporal evolution of the heat fluxes involved in the budget are presented in the Fig. 9 for the different investigated distance parameters. As expected, the term (a) corresponding to the droplet heating depends not on the distance parameter, since an unique temperature profile has been retained, except for $C = 2.6$. This flux vanished when the equilibrium temperature is reached. The vaporization heat flux depends not strongly on the time and is mainly governed by the aerodynamic interactions according to the modified D^2 law, since a noticeable dependence on the distance parameter is observed, as mentioned in numerous papers [7,19]. The convection heat flux depends both on time and distance parameter. The distance parameter dependence is due to the nature of the convective heat exchange itself, which is dependent on the nature of the flowfield, related to the aerodynamics interactions. The convective heat exchange is enhanced as the distance parameter is increased, due to the reduction of the volume of the entrained air column. As far as the temporal evolution of the convection heat flux is concerned, two main phases can be distinguished. A first phase where the convective heat flux is almost constant, corresponding to the heating phase of the droplets (from 0 to 6 ms), followed by an intermediate phase where the flux decreases to a constant value corresponding to the equilibrium. These experiments suggest that two heat transfer coefficients could be defined, one corresponding to the heating phase, the other to the equilibrium phase where the energy gained by convection compensates the losses by vaporization, both depending on the distance parameter. This change in the heat transfer coefficient should be related to a modification of the aerodynamic regime in the droplet stream boundary layer and will be discussed in the Section 4.5. The intermediate phase could correspond to the transition from one phase to the other, but remains difficult to interpret quantitatively, since very few measurements have been performed in this zone (see the temperature profile, in the Fig. 8). Each phase has been limited in time as follows:

- strong heating (0, 4.5 ms)
- intermediate (4.5, 8 ms)
- equilibrium (8, 11 ms)

The Fig. 10 summarized the results obtained about the convective heat flux as a function of the distance parameter, for both heating and equilibrium phases. The heat flux is about 60% higher in the heating phase than in the equilibrium phase. The distance parameter influence is the strongest between $C = 2$ and 8 and decreases clearly after, as already observed for the evaporation rate (see Fig. 7). The convective heat transfer coefficient h, calculated by the relation $\Phi_{\mathrm{c}} = hS(T_{\infty} - T_{\mathrm{S}})$, approximated by $\Phi_{\mathrm{c}} \simeq hS(T_{\infty} - T_{\mathrm{m}})$, is represented in the Fig. 11, follows the same tendency. It is higher in the heating

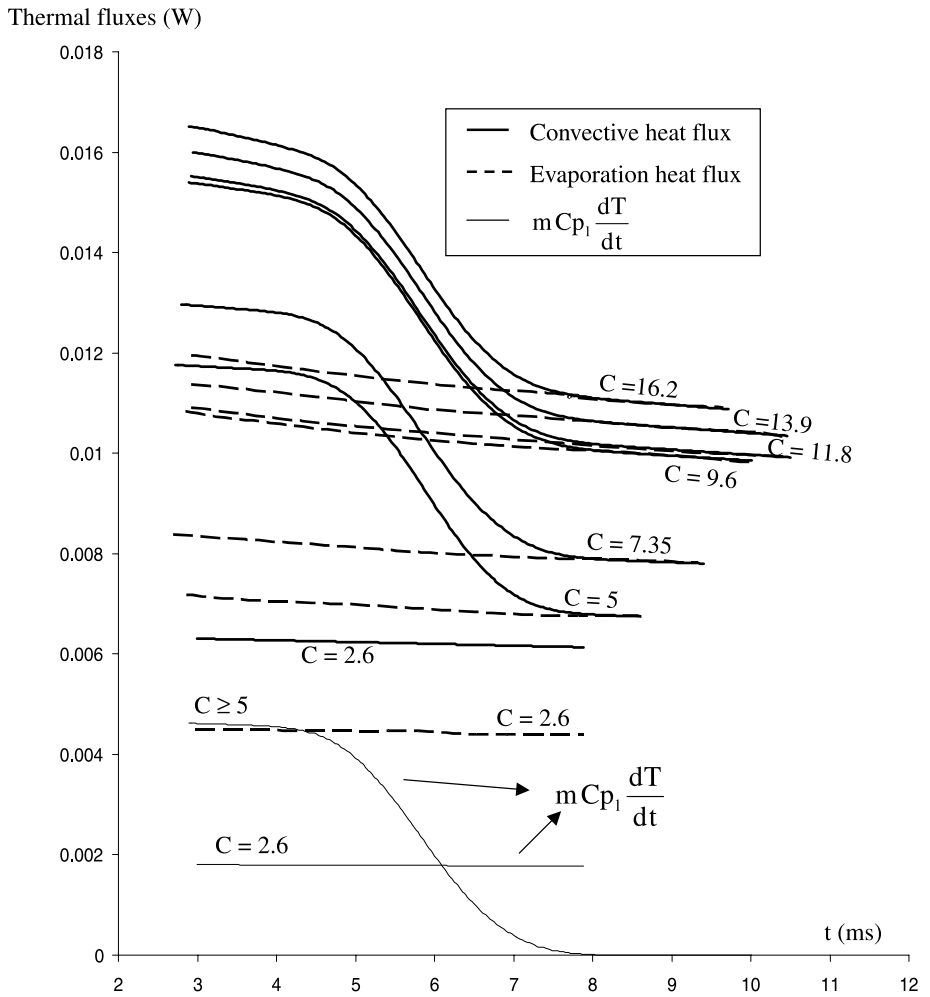

Fig. 9. Temporal evolution of the fluxes involved in the droplet thermal budget.

phase, where it evolves from $h = 600\ \mathrm{W\,m^{-2}\,K^{-1}}$ to $h = 1500\ \mathrm{W\,m^{-2}\,K^{-1}}$, as it evolves from $700\ \mathrm{W\,m^{-2}\,K^{-1}}$ to about $1200\ \mathrm{W\,m^{-2}\,K^{-1}}$ in the equilibrium phase (Fig. 11). It should also be noted that the distance parameter evolution range is shorter in the equilibrium phase, due to the inter-droplet distance decrease. According to the uncertainties on the measurements of the sizes and temperatures, the estimated uncertainty on the determination of the convection coefficient h is about 20%.

4.4. Nusselt number and comparisons

The experimental determination of the convection heat transfer coefficient enables to calculate the Nusselt number. The gas phase conductivity calculated at the reference state and the measured droplet diameter are used. The Nusselt number evaluation as a function of the distance parameter is presented in the Fig. 12, for both heating and equilibrium phases. The Nusselt number growths as C is increased from about 2–7 for the heating phase and to about 2–6 for the equilibrium phase. After, the increase is much lower, tending to an asymptotic behavior. The Nusselt number seems to stabilize at about 5.5 for the heating phase and about 3.5 for the equilibrium. This should be compared to numerical previous works on both isolated droplets [3] and interacting droplets [5], with evaporation. Chiang et al. [3] performed the numerical simulation of the heat transfer of a moving evaporating isolated droplet, also reported in the Fig. 12, in the heating phase of the droplet, with inclusion of a model for the internal droplet heat diffusion. The Nusselt numbers of an isolated droplet should not present any variations with the distance parameter, but the slow represented variations are due to adjustments performed in order to reach conditions corresponding to interacting droplets with

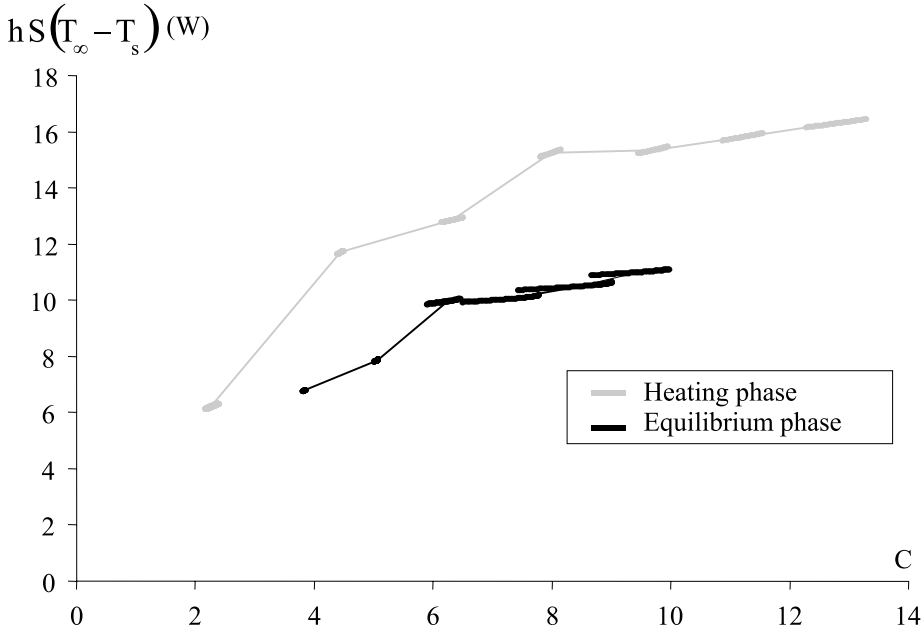

Fig. 10. Convective heat flux temporal evolution.

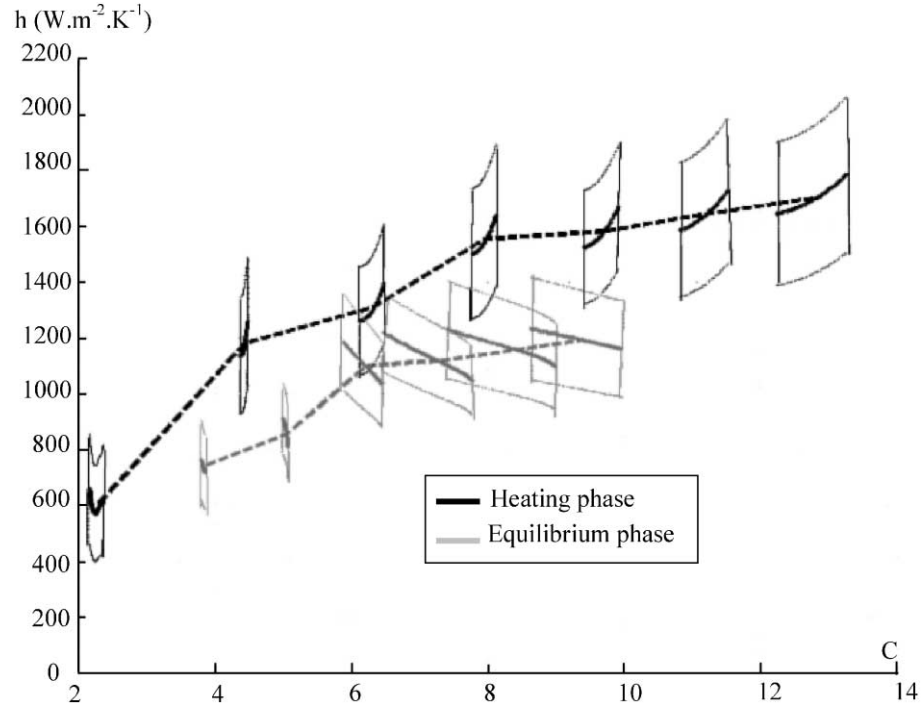

Fig. 11. Convection heat transfer coefficient evolution as a function of the distance parameter.

similar conditions on the diameter and the gas phase properties. It is clearly observed that the Nusselt number determined experimentally in the droplet heating phase seems to coincide with the numerical simulations of Chiang et al. [3] for high distance parameters, where interaction phenomena are less sensitive, which can be

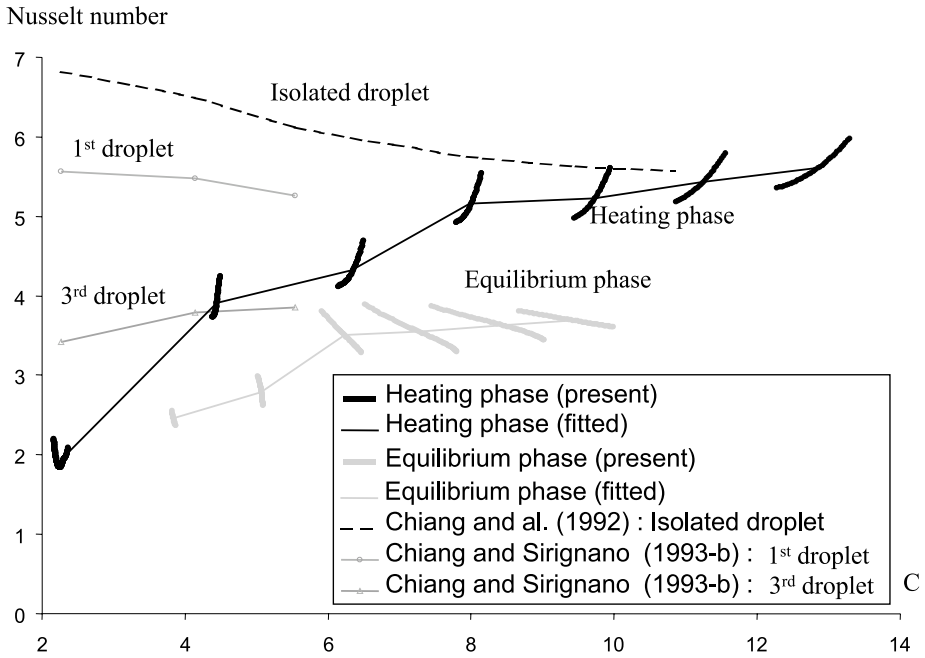

Fig. 12. Nusselt number evolution as a function of the distance parameter and comparison with literature.

considered as a good validation of the approach undertaken in the present work. The comparison with the simulations of Chiang and Sirignano [5], for three droplets in linear stream appears also interesting: this simulation is performed for distance parameters exceeding not 6 and for very short characteristic times, corresponding to the droplets' heating phase, for the first and third droplet. For distance parameters varying from 4 to 6, the experimental Nusselt numbers, determined in the heating phase, are in reasonable agreement with those calculated for the third droplet. The agreement is bad for $C < 4$, where the aerodynamic interactions are the strongest, showing that a three droplets arrangement is not sufficient to take into account these interactions. No comparisons can be performed for the Nusselt number determined in the equilibrium phase, since the characteristic times of the numerical simulations available in the literature are too short and corresponds to the heating phase.

4.5. Interpretation of the mechanisms

The evaporation rate is governed by the aerodynamics interactions and by the diffusive mechanisms in the gaseous phase through the modified D^2 law: the fuel vapor mass fraction Y_S is fixed at the droplet surface by these different mechanisms. Assuming that the gaseous layer in the immediate vicinity of the droplet surface is in the saturation conditions, the surface temperature is imposed by the equilibrium fuel mass fraction Y_S, through the Clausius–Clapeyron law. The evaporation rate is directed by the vapor advection and diffusion mechanisms in the droplet stream boundary layer, which should present a strong dependence on the interaction regime. Since this law is exponential in the considered temperature range, a large variation of Y_S with time or with the distance parameter, is associated to a moderate variation of the surface temperature T_S. Considering that the droplets are injected at 46 °C, it can be assumed that the equilibrium droplet surface temperature is established very soon in the heating phase of the droplet, probably a few ms after injection, and is almost independent on the distance parameter. Consequently, the observed heating time corresponds to the heat diffusion within the droplet, resulting from pure conduction in the liquid fuel and from convection due to the formation of internal vortices. Only the second heat diffusion mode by convection should depend on the aerodynamic interactions. The effective conductivity model described by Abramzon and Sirignano [20] allows to take into account the internal convection phenomena by multiplying the fuel conductivity by a factor χ, depending on the droplet Peclet number, resulting in an equivalent conductivity. The calculation of the Peclet number has been performed using the model of Abramzon and Sirignano [20]. The factor χ value is about 2.72 and is completely insensitive to the distance parameter in the considered range. It should not affect significantly the heat conduction time and the unique temperature profile observed for the droplet temperature can be interpreted in

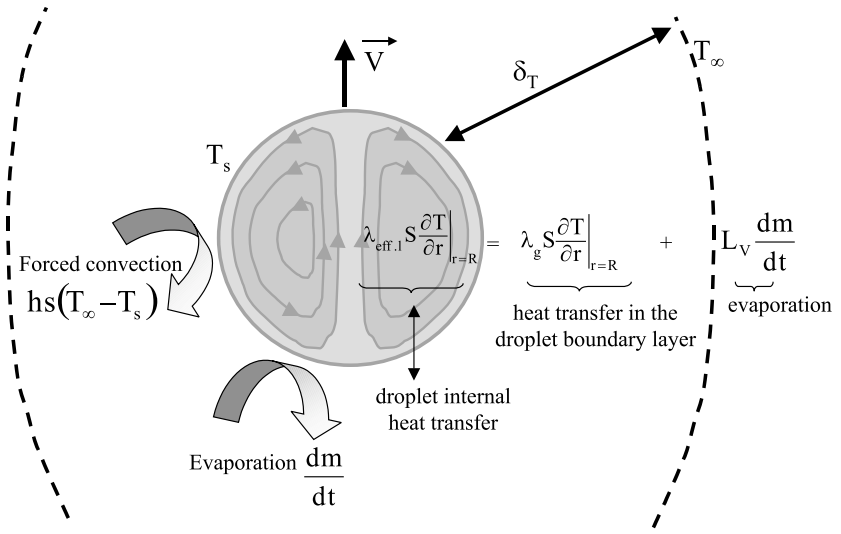

Fig. 13. Sketch of the heat fluxes in the droplet environment.

the light of the heat diffusion within the droplet, which appears non-dependent on the distance parameter. When $C \geqslant 5$, the characteristic heating time of the droplet appears directed by the efficiency of the droplet internal heat transfer by combined conduction and convection. The maximum heat flux transferred to the droplet corresponds to the case for which the droplet surface is imposed at the equilibrium temperature from the first instants of the heating. At the droplet surface, the heat flux conducted in the thermal boundary layer, provided by the forced convection heat transfer, is partly used for the evaporation and partly for heating the droplet (Fig. 13):

$$\underbrace{\lambda_g S \left.\frac{\partial T}{\partial r}\right|_{r=R_d}}_{\text{gas (a)}} = \underbrace{\lambda \text{eff}_l S \left.\frac{\partial T}{\partial r}\right|_{r=R_d}}_{\text{liquid (b)}} - L_v \frac{dm}{dt} \qquad (1.12)$$

When the droplet temperature is homogeneous, after the completion of the heating phase, the heat flux transferred to the droplet is null, as the flux associated to the vaporization remains almost constant. Consequently, the heat flux associated to the gaseous phase $\lambda_g S \frac{\partial T}{\partial r}|_{r=R_d}$ decreases in parallel with the temperature gradient in the vicinity of the droplet surface, meaning that the thermal boundary layer of the droplet thickens. The convective heat transfer coefficient can be defined by:

$$hS(T_\infty - T_S) \sim \lambda_g S \frac{(T_\infty - T_S)}{\delta_T} \qquad (1.13)$$

where δ_T is the droplet stream boundary layer thickness. The Eq. (1.13) shows that the decrease of the convective heat transfer coefficient is in good accordance with the assumed increase of the boundary layer thickness.

For low distance parameters, as in the case of $C = 2.6$, the heating phase appears much longer than in the case of distance parameters higher than 5. It may be assumed that the convective heat flux is not sufficient to ensure both evaporation and droplet heating. Furthermore, it may be assumed that the heat diffusion phenomena are less efficient under a so strong interaction regime. The heat flux transferred to the droplet (term (b)) is lower than in the case $C \geqslant 5$. According to Eq. (1.12), since the effective liquid conductivity may not present variations with the interaction regime, the heat flux provided by the gaseous phase is now the limiting factor. In this case, the equilibrium temperature is equal to these measured for the higher distance parameters, but the heating time is longer since the surface temperature is continuously increasing during the heating phase. However, no measurements can be performed in the equilibrium phase, since droplets collisions occur far from the injection point for such small distance parameters. The highest measured temperature is about 55 °C, where measurements remain possible, which is not far from the equilibrium temperature of 60 °C, which appears in favor of this hypothesis.

5. Conclusions

The combination of two optical techniques has enabled to measure on the same experiment the droplet size and temperature. With the use of these techniques, both droplet heating and evaporation rate can be quantified. The overall thermal budget determined on an evaporating monodisperse stream, injected in the thermal boundary layer of an heated vertical plate allowed

to determine the convective heat transfer term and the subsequent heat transfer coefficient. Two phases are highlighted: the first one corresponding to the droplet heating and the second one to an equilibrium phase, where the droplets vaporize at constant and uniform temperature. This heat convection coefficient appears higher in the heating phase than in the equilibrium and strongly dependent to the inter-droplet distance in both phases. The Nusselt number, evaluated for both has been evaluated as a function of the distance parameter. The results obtained are consistent with the current models of isolated droplets for the large distance parameters, where aerodynamic interactions are strong. However, corrections of the Nusselt numbers have to be applied for the smallest distance corresponding to strong interaction regimes. For distance parameters higher than 5, the droplet heating time is limited by the heat diffusion mechanisms within the droplet, as it is limited by the heat flux transferred from the gaseous phase to the liquid for smaller distance parameters. It demonstrates the high interest to investigate the droplet internal heat diffusion phenomena by measuring the temperature distribution within the droplet. Hypothesis about the mechanisms have been formulated, but some additional data about the gaseous phase such as fuel vapor concentration distribution in the droplet stream vicinity and about both dynamic and thermal boundary layers are necessary in order to validate these assumptions.

References

[1] G.B. Wallis, One-dimensional two-phase flows, McGraw-Hill, New York, 1969.
[2] D.B. Spadling, The combustion of liquid fuels, in: Fourth international Symposium on Combustion, Williams and Wilkins, Baltimore, 1953, p. 847.
[3] C.H. Chiang, M.S. Raju, W.A. Sirignano, Numerical analysis of convecting, vaporizing, fuel droplet with variable properties, Int. J. Heat Mass Transfer 35 (1992) 1307.
[4] C.H. Chiang, W.A. Sirignano, Interacting, convecting, vaporizing fuel droplets with variable properties, Int. J. Heat Mass Transfer 36 (1993) 875.
[5] C.H. Chiang, W.A. Sirignano, Axisymmetric calculation of three-droplets interactions, Atomization Sprays 3 (1993) 9.
[6] J.F. Virepinte, Etude du comportement dynamique et thermique de gouttes en régime d'interaction dans le cas de jets rectilignes, Ph.D. Thesis, Ecole Nationale Supérieure de l'aáronautique et de l'Espace, 1999.
[7] J.F Virepinte, Y. Biscos, G. Lavergne, P. Magre, G. Collin, A rectilinear droplet stream in combustion: droplet and gas phase properties, Combust. Sci. Technol. 150 (2000) 143.
[8] G. Koenig, K. Anders, A. Frohn, A new light scattering technique to measure droplet diameter of periodically generated moving droplets, J. Aerosol Sci. 17 (1986) 157.
[9] P. Lavieille, F. Lemoine, G. Lavergne, M. Lebouché, Evaporating and combusting droplet temperature measurements using two colors laser-induced fluorescence, Exp. Fluids 31 (2001) 45.
[10] J. Van Beeck, M. Riethmuller, Non-intrusive measurements of temperature and size of single falling raindrops, Appl. Opt. 34 (1995) 1633.
[11] N. Roth, K. Anders, A. Frohn, Refractive index measurements for the correction of particle sizing methods, in: 2nd International Congress on Optical Particle Sizing, Arizona State University, Tempe, USA, 1990.
[12] P. Massoli, Rainbow refractometry applied to radially inhomogeneous spheres: the critical case of evaporating droplets, Appl. Opt. 37 (1998) 3227.
[13] F. Lemoine, Y. Antoine, M. Wolff, M. Lebouché, Simultaneous temperature and 2D velocity measurements in a turbulent heated jet using combined laser-induced fluorescence and LDA, Exp. Fluids 26 (1999) 315.
[14] G.A.E. Godsave, Studies of the combustion of drops in a fuel spray: The burning of single drops of fuel, in: Fourth International Symposium on Combustion, Williams and Wilkins, Baltimore, USA, 1953, p. 818.
[15] W.E. Ranz, W.R. Marshall, Evaporation from drops, Chem. Eng. Prog. 48 (1952) 173.
[16] M. Labowsky, Calculation of the burning rates of interacting fuel droplets, Combust. Sci. Technol. 22 (1980) 217.
[17] G.L. Hubbard, V.E. Denny, A.F. Mills, Droplet evaporation: effects of transient and variable properties, Int. J. Heat Mass Transfer 18 (1975) 1003.
[18] C.K. Law, Recent advances in droplet vaporization and combustion, Prog. Energy Combust. Sci. 8 (1982) 171.
[19] M.A. Silverman, D. Dunn-Rankin, Experimental investigation of a rectilinear droplet stream flame, Combust. Sci. Technol. 100 (1994) 57.
[20] B. Abramzon, W.A. Sirigiano, Droplets vaporization model for spray combustion calculations, Int. J. Heat Mass Transfer 32 (1989) 1605.